chemistry

MDPI

Article

Nitrogen-Doped MXene Electrodes for High-Voltage Window Supercapacitors in Organic Electrolytes

Yingyi Liao †, Xiaoqing Bin †, Jing Xu, Xuedong He and Wenxiu Que *

Electronic Materials Research Laboratory, Key Laboratory of the Ministry of Education, International Center for Dielectric Research, Shaanxi Engineering Research Center of Advanced Energy Materials and Devices, School of Electronic Science and Engineering, Xi'an Jiaotong University, Xi'an 710049, China; liaoll@stu.xjtu.edu.cn (Y.L.); heloise77@stu.xjtu.edu.cn (X.B.); 3123153019@stu.xjtu.edu.cn (J.X.); xuedonghe@stu.xjtu.edu.cn (X.H.)

* Correspondence: wxque@xjtu.edu.cn

† These authors contributed equally to this work.

Abstract: MXene has excellent electrochemical performance in aqueous electrolytes; however, its narrow voltage window (hydrolysis voltage $\leq$ 1.2 V) limits the energy density of supercapacitors. Compared to conventional aqueous electrolytes, ionic liquid (IL) electrolytes exhibit a much larger voltage window, but their larger ion size limits the transport and intercalation of IL cations in MXene electrodes. Therefore, the electrochemical performances for three different types of organic electrolytes based on nitrogen-doped MXene electrodes in supercapacitors were investigated, with the voltage windows of the devices effectively widened to 2.4 V. In addition, the nitrogen-doped MXene electrodes also effectively adjusted the interlayer spacing of the MXene nanosheets, with the enlarged interlayer spacing (from 12.60 Å to 14.24 Å) being more favorable for the intercalation and de-intercalation of larger-sized organic ions within the electrodes, thus effectively storing a charge. Among them, the 1 M EMIMTFSI/LiTFSI/ACN electrolyte is optimal due to the introduction of a smaller ion size for Li^+, and so the corresponding supercapacitor achieves the electrode capacitance of up to 147 F g^{-1}, with the maximum energy density of 29.4 Wh kg^{-1}. This work provides a new strategy for reasonably optimizing the design of organic electrolytes matching modified MXene electrodes to effectively enhance the energy density of supercapacitors.

Keywords: MXene; nitrogen doped; ionic liquid; high-voltage window; supercapacitors

check for updates

Academic Editor: Michael Lyons

Received: 14 December 2024
Revised: 17 January 2025
Accepted: 21 January 2025
Published: 23 January 2025

Citation: Liao, Y.; Bin, X.; Xu, J.; He, X.; Que, W. Nitrogen-Doped MXene Electrodes for High-Voltage Window Supercapacitors in Organic Electrolytes. *Chemistry* **2025**, *7*, 13. https://doi.org/10.3390/chemistry7010013

Copyright: © 2025 by the authors. Licensee MDPI, Basel, Switzerland. This article is an open access article distributed under the terms and conditions of the Creative Commons Attribution (CC BY) license (https://creativecommons.org/licenses/by/4.0/).

1. Introduction

Among the various energy storage devices, supercapacitors (SCs) have gained substantial attention due to their high power density, long cycle life, and rapid charge–discharge rates [1]. However, their relatively low energy density compared to batteries has hindered their broader application [2]. To overcome this challenge, it is essential to match electrode materials with excellent capacitance to the compatibility with large-voltage window electrolytes [3].

MXene, a novel family of two-dimensional transition metal carbides, nitrides, and carbonitrides, emerged in 2011 [4]. MXene exhibits unique structural and chemical properties, including excellent electrical conductivity, a high specific surface area, and the ability to host cations of different sizes. It has also shown potential in electrode materials [5,6]. Lukatskaya et al. demonstrated that $Ti_3C_2T_x$ MXene hydrogels delivered volumetric capacitance similar to 1500 F cm^{-3} in H_2SO_4 electrolyte [7]. However, the low decomposition

voltage of water presents a significant obstacle to achieving devices with high energy density [8].

Unlike aqueous electrolytes, organic electrolytes can operate over a much wider voltage range and enable higher energy densities, especially ionic liquids (ILs) electrolytes [9]. In addition, ionic liquids also have the characteristics of high chemical stability, suitable viscosity at non-low temperature, and high conductivity [10]. Imidazolium cations and tetraalkylammonium cations are types of IL cations used in supercapacitors [11,12]. Moreover, several studies have reported the electrochemical performance of $Ti_3C_2T_x$ MXene in ionic liquid electrolytes [13–15]. The results indicate that the use of organic ionic liquid electrolytes with larger ion sizes(0.75–1.4 nm) hinders the intercalation and de-intercalation of their cations within the MXene interlayers. Dall' Agnese et al. reported that the capacitance of multilayer MXene in 1M 1-ethly-3-methylimidazolium bis-(trifluoromethyl sulfonyl)-imide (EMIMTFSI) in acetonitrile (ACN) is increased from 35 F g^{-1} to 85 F g^{-1} [13]. Lin et al. reported a capacitance of 70 F g^{-1} using a $Ti_3C_2T_x$ ionogel electrode in a neat EMIMTFSI electrolyte [15]. Researchers have realized that larger interlayer-spaced MXene can achieve better electrochemical performance in IL [16,17]. In addition, a strategy involves introducing redox active components into ionic liquid electrolytes to enable the MXene-based electrodes of faster Faradaic reactions to contribute to the pseudocapacitance, thus obtaining a higher energy density [18,19]. Nitrogen doping is an effective approach to achieving the better electrochemical performance of MXene by influencing the electronic transmission process [20,21]. Here, urea acts as an N-doping source, and ethanol acts as an auxiliary organic solvent.

In this work, we synthesized freestanding and compact N-doped delaminated d-$Ti_3C_2T_x$ (UN-$Ti_3C_2T_x$) film electrodes, and investigated their electrochemical performance in three different electrolytes, including 1 M EMIMTFSI/NaTFSI/ACN, 1 M $(C_4H_9)_4N(ClO_4)$/NaTFSI/ACN, and 1 M EMIMTFSI/LiTFSI/ACN electrolytes, respectively. As a result, the symmetric supercapacitor was capable of operating with a 2.4 V voltage window in three different organic electrolytes. Specifically, in the 1 M EMIMTFSI/LiTFSI/ACN electrolyte, the UN-$Ti_3C_2T_x$ film electrode exhibits a remarkable specific capacitance of 147 F g^{-1} at 0.5 A g^{-1} and the corresponding device shows a well enough energy density of 29.4 Wh kg^{-1} at a power density of 600 W kg^{-1}. To summarize, the ILs can provide a higher voltage window and nitrogen-doped MXene electrodes can improve interlayer spacing. The strategy of using organic ionic liquids as electrolytes matched with the modified nitrogen-doped MXene electrodes properly can effectively enhance the energy density of supercapacitors. Figure 1 is the schematic diagram for a supercapacitor in the 1 M EMIMTFSI/LiTFSI/ACN electrolyte based on nitrogen-doped MXene electrodes.

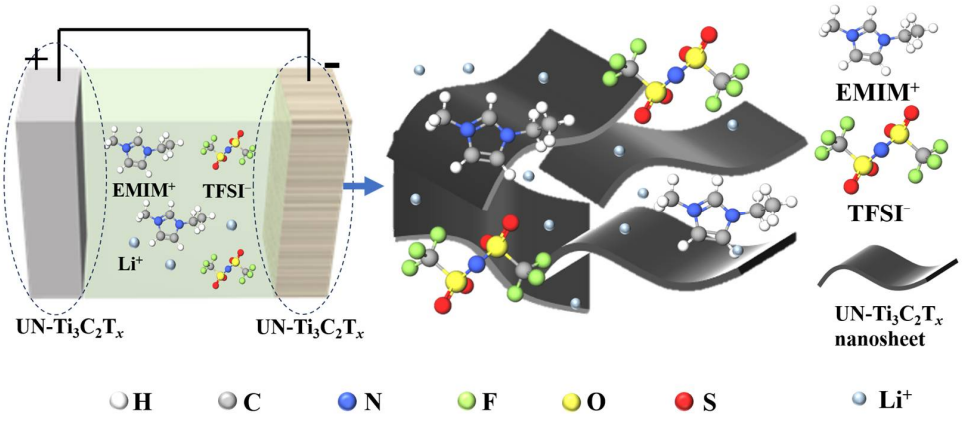


Figure 1. Schematic diagram for supercapacitor in 1 M EMIMTFSI/LiTFSI/ACN electrolyte based on nitrogen-doped MXene electrodes.

2. Materials and Methods

2.1. Synthesis of Ti_3AlC_2 Powders

The Ti_3AlC_2 was prepared by a vacuum sintering method, which mixed all powders of TiC, Al, and Ti in a molar ratio of 2:1.2:1. The mixed powders were milled in a mortar with ethyl alcohol for 30 min, and dried in the oven at 60 °C for 4 h. Then, the mixture was annealed in an alundum tube in Ar gas at a flow rate of 100 mL min^{-1}. The heating curve involves heating at a rate of 10 °C min^{-1} from room temperature to 500 °C, then at 8 °C min^{-1} to 900 °C, and finally at 6 °C min^{-1} to 1350 °C, then holding at 1350 °C for 2 h. After the reaction was completed, the Ti_3AlC_2 ceramic block was thus obtained. Then, it was ground by a stainless steel mortar and sieved through a 400 mesh screen. The Ti_3AlC_2 powders were obtained for further study.

2.2. Synthesis of $Ti_3C_2T_x$ MXene

The $Ti_3C_2T_x$ MXene film (d-$Ti_3C_2T_x$) was synthesized by selective etching MAX followed by delamination [22]. Firstly, 2 g of LiF was added to 20 mL of 9 M HCl aqueous solution, stirring for 10 min. Then, 1 g of Ti_3AlC_2 powder was put slowly into this, and the solution was allowed to stir at 38 °C for 24 h. After that, deionized (DI) water was used to repeatedly wash the etchant mixture, followed by centrifugation at 5000 rpm for 5 min in each cycle, until the pH value was higher than 7. The obtained multilayered $Ti_3C_2T_x$ sediment was dispersed with DI water, which was deoxidized using vacuum evacuation, followed by ultrasonicating for 1 h, and centrifuging for 30 min at 3500 rpm. The suspension was collected for further use. Finally, a certain volume of the suspension was vacuum-filtrated and slowly dried at 45 °C; thus, the concentration of $Ti_3C_2T_x$ aqueous solution can be known.

2.3. Nitrogen Doping of Few-Layer d-$Ti_3C_2T_x$ Flakes (UN-$Ti_3C_2T_x$ Films)

Firstly, 10 mL of d-$Ti_3C_2T_x$ suspension with a known concentration and 35 mL of absolute ethanol were added into the 50 mL centrifuge tube and centrifuged at 8000 rpm for 5 min, which decanted the supernatant. Then, the d-$Ti_3C_2T_x$ suspension and absolute ethanol were added to the base of sediment repeatedly, shaken, and centrifuged, until the mass of d-$Ti_3C_2T_x$ was calculated to be about 40 mg. The sediment was collected to obtain few-layer d-$Ti_3C_2T_x$ nanosheets. Then, 20 mL of urea saturated alcohol solution was added into the as-prepared few-layer d-$Ti_3C_2T_x$ sediment, which was shaken and rotated, then transferred to a 50 mL Teflon container, and added with 2 g of urea again to maintain an adequate nitrogen atmosphere. After stirring for 30 min, the 50 mL Teflon container was placed into a corresponding stainless-steel autoclave reactor and heated at 200 °C for 24 h in a drying oven. After cooling, the solid residue was washed and centrifuged with ethanol (3 cycles) and ultrapure water (2 cycles). After the last centrifugation, 30 mL of ultrapure water was added into the N-doped $Ti_3C_2T_x$ flake sediment, which was shaken and rotated for 10 min, and ultrasonicated for 30 min, followed by vacuum filtration and drying in air at room temperature; thus, the urea-assisted N-doped UN-$Ti_3C_2T_x$ film was obtained.

2.4. The Preparation for Organic Electrolytes

1 M EMIMTFSI/NaTFSI/ACN, 1 M $(C_4H_9)_4N(ClO_4)$/NaTFSI/ACN, and 1 M EMIMTFSI/LiTFSI/ACN were used as organic electrolytes. For the 1 M EMIMTFSI/LiTFSI/ACN electrolyte, firstly, 2.56 mL of EMIMTFSI and 2.87 g of LiTFSI were dissolved in 7.44 mL of acetonitrile (ACN) (malor ratio of EMIMTFSI: LiTFSI: ACN = 1:1:1), then, stirred for 2 h. For comparative purposes, 1 M EMIMTFSI/NaTFSI/ACN and 1 M $(C_4H_9)_4N(ClO_4)$/NaTFSI/ACN were prepared by the same molar ratio and method. For 1 M EMIMTFSI/NaTFSI/ACN, 2.56 mL of EMIMTFSI and 3.03 g of NaTFSI were dis-

solved in 7.44 mL of acetonitrile (ACN). For 1 M $(C_4H_9)_4N(ClO_4)$/NaTFSI/ACN, 3.42 g of $(C_4H_9)_4N(ClO_4)$ and 3.03 g of NaTFSI were dissolved in 10 mL of acetonitrile (ACN).

2.5. Morphology and Structure Characterizations

Scanning electron microscopy (SEM) images of the samples were observed by using JSM-390 from JEOL Inc. X-ray diffraction (XRD) patterns of the samples were tested by using a Rigaku D/max 2200pc diffractometer with Cu radiation.

2.6. Electrochemical Measurements

Electrochemical performance tests such as cyclic voltammetry (CV), galvanostatic charge–discharge (GCD), and electrochemical impedance spectra (EIS) were carried out using a CHI660E workstation (CH Instruments, Shanghai, China). The electrochemical performance test of a symmetric supercapacitor was measured by a two-electrode system. The UN-$Ti_3C_2T_x$ films were punched into disks and used as cathode and anode electrodes. 1 M EMIMTFSI/NaTFSI/ACN, 1 M $(C_4H_9)_4N(ClO_4)$/NaTFSI/ACN, and 1 M EMIMTFSI/LiTFSI/ACN were used as electrolytes, respectively. Based on the potential-time profile (galvanostatic test), the specific capacitance (C, F g^{-1}), the energy density (E, Wh kg^{-1}), and the power density (P, W kg^{-1}) for supercapacitors were calculated by the following equations:

$$C = \frac{I * \Delta t}{\Delta U * m}$$

where C implies the specific capacitance (F g^{-1}) of the cell; I indicates the discharge current (A); Δt is the discharge time (s); m is the total mass (g) of active material; and ΔU represents the voltage window (V).

$$E = \frac{1}{2}\frac{C\Delta U^2}{3.6}$$

$$P = 3600\frac{E}{\Delta t}$$

where C implies the specific capacitance (F g^{-1}) of the cell; ΔU represents the voltage window (V); and Δt is the discharge time (s); E is energy density and P is power density.

3. Results and Discussion

3.1. Structure and Morphological Analysis

The surface and cross-sectional morphological properties of the d-$Ti_3C_2T_x$ MXene and UN-$Ti_3C_2T_x$ MXene films were characterized by scanning electron microscopy (SEM), and the results are shown in Figure 2. Figure 2a,b show the low-magnification and high-magnification SEM images for the d-$Ti_3C_2T_x$ film; it can be observed that both of them have relatively smooth surface morphologies. And, Figure 2c exhibits the layer structure for the $Ti_3C_2T_x$ film. Then, after the introduction of nitrogen, there are more wrinkles and complexities on the surface for the UN-$Ti_3C_2T_x$ film (Figure 2d,e). Urea acts as an N-doping source and alcohol as a solvent has a smaller molecule size, low viscosity, and high mobility, which can greatly improve the diffusion of the urea molecule, and thus avoids destroying the layered structure for MXene. As shown in Figure 2f (cross-section view of the UN-$Ti_3C_2T_x$ film), the layered structure of the UN-$Ti_3C_2T_x$ MXene flakes can be still observed. The elemental mappings of the UN-$Ti_3C_2T_x$ film (Figure 2g–j) show the presence and homogeneous distribution of Ti, C, O, and N elements, which further proves the successful preparation of the UN-$Ti_3C_2T_x$ film.

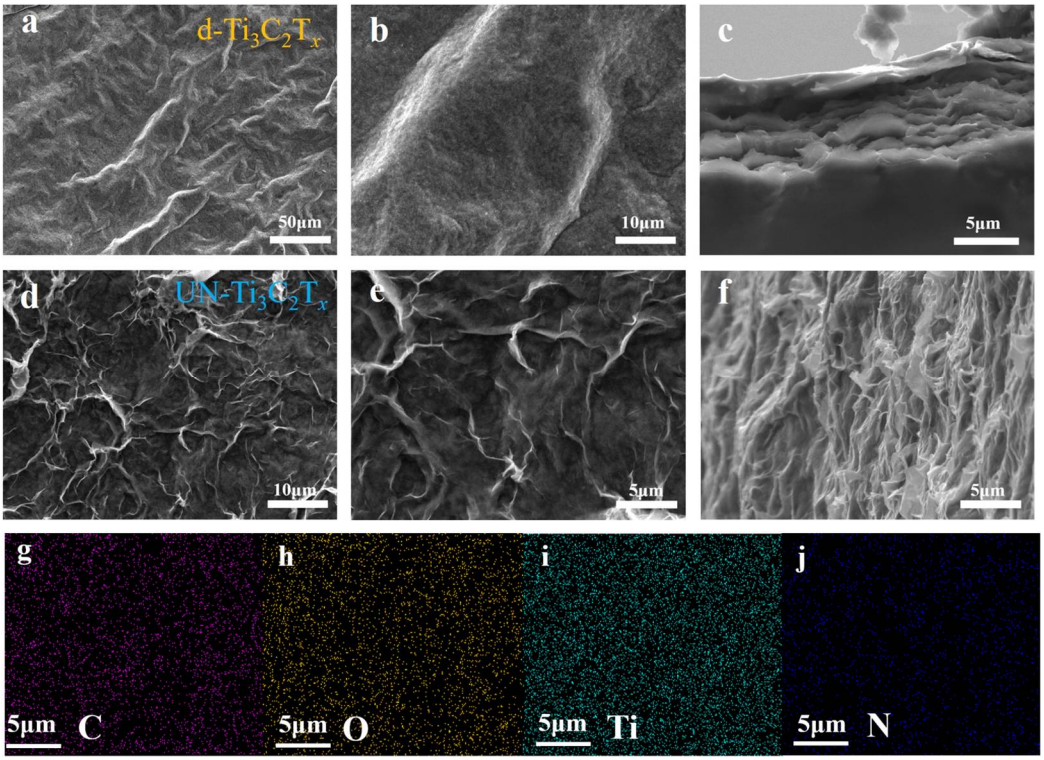


Figure 2. SEM images of the surface of the (**a**,**b**) d-$Ti_3C_2T_x$ film, and the (**d**,**e**) UN-$Ti_3C_2T_x$ film. SEM for a cross-section view of the (**c**) d-$Ti_3C_2T_x$ and (**f**) UN-$Ti_3C_2T_x$ films. (**g**–**j**) EDS elemental mappings of Ti, C, N, and O elements for UN-$Ti_3C_2T_x$ film.

XRD measurement could effectively reveal the results of Al etching. As shown in Figure S1 (Supporting Information), there is a set of characteristic peaks of the Ti_3AlC_2 phase. After the LiF/HCl solution etching treatment and exfoliation, all the peaks in the Ti_3AlC_2 pattern except the (002) peak disappeared compared to the XRD pattern of d-$Ti_3C_2T_x$ (Figure 3a), and the (002) peak shift to lower angles, implying that the Al layer has been well etched and that the Ti_3AlC_2 powders have successfully transformed into $Ti_3C_2T_x$ MXene nanosheets.

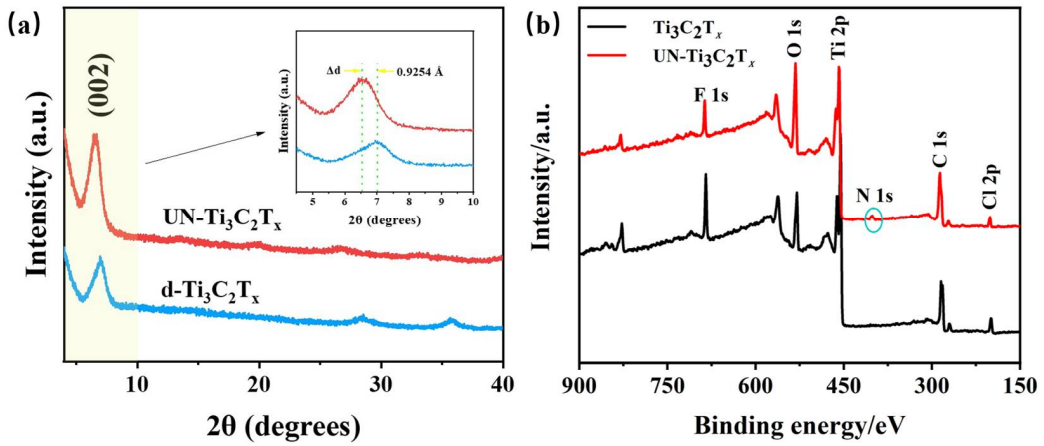


Figure 3. (**a**) XRD patterns of the d-$Ti_3C_2T_x$ and UN-$Ti_3C_2T_x$ film samples. The inset shows the diffraction peaks at around the (002) lattice plane and the corresponding interlayer spacing difference (Δd) of the film samples, and the (**b**) XPS spectra of the d-$Ti_3C_2T_x$ and UN-$Ti_3C_2T_x$ film samples.

Figure 3a shows the XRD patterns of the d-$Ti_3C_2T_x$ and UN-$Ti_3C_2T_x$ film samples. As seen in Figure 3a, after an introduction of nitrogen, the (002) diffraction peak is discovered to offset to a lower angle for the UN-$Ti_3C_2T_x$ film, which agrees well with the previous studies [23]. It can be observed from the inset that the (002) peak is shifted from 7.01° of d-$Ti_3C_2T_x$ to 6.53° of UN-$Ti_3C_2T_x$, and the corresponding d-spacing changes from 12.60 Å to 14.24 Å, illustrating the successful substitution of the nitrogen elements in the urea molecule for carbon elements in d-$Ti_3C_2T_x$. And, the increased interlayer spacing contributes to the intercalation and transport of larger-sized ions, thus effectively storing charge.

XPS is a widely used spectroscopic technique for the study of the element valence. Figure 3b shows XPS spectra of the d-$Ti_3C_2T_x$ and UN-$Ti_3C_2T_x$ film samples. It can be observed that the spectra of both samples exhibit signals for Ti 2p, C 1s, O 1s, F 1s, and Cl 2p. Specifically, the N 1s signal is detected in the UN-$Ti_3C_2T_x$ film, indicating the successful doping of the nitrogen element into the d-$Ti_3C_2T_x$ layers. As presented in Table S1 (Supporting Information), the N content of the UN-$Ti_3C_2T_x$ film is 2.17%, causing defects that act as active sites to provide pseudocapacitive performance. And, the F content decreases from 11.02% to 6.47%, and it has been reported in the literature that the reduction in F content is beneficial for improving capacitance [24].

Studies have shown [25] that the introduction of nitrogen atoms creates new active sites in the lattice structure of MXene. These active sites can adsorb more charges, thereby enhancing the charge storage capacity of MXene. In addition, nitrogen-containing functional groups can accelerate ion transport, improve surface wettability (increase the number of active sites), and provide Faradaic reaction dynamics for additional capacity, thereby significantly enhancing the electrochemical performance of the material. Hence, the UN-MXene film is expected to have an enhanced electrochemical performance.

3.2. Electrochemical Performance Testing

The electrochemical performance was studied by a two-electrode symmetric Swagelok cell, and 1 M EMIMTFSI/LiTFSI/ACN, 1 M EMIMTFSI/NaTFSI/ACN and 1 M $(C_4H_9)_4N(ClO_4)$/NaTFSI/ACN were used as electrolytes. The corresponding CV curves of the UN-$Ti_3C_2T_x$ films in three types of electrolytes at a scan rate of 20 mV s^{-1} are shown in Figure 4a, and they all show a quasirectangular shape with partial redox peaks in a voltage window of 0–2.4 V. In general, smaller-sized ions are beneficial for the intercalation and de-intercalation of ions within the electrodes to store charges. More specifically, it is noted that the current density in the CV curves of the UN-$Ti_3C_2T_x$ film in the 1 M EMIMTFSI/LiTFSI/ACN electrolyte is higher than the those in other electrolytes (1 M EMIMTFSI/NaTFSI/CAN and 1 M $(C_4H_9)_4N(ClO_4)$/NaTFSI/ACN), suggesting its higher specific capacitance. Also, as observed in Figure 4b,c, the discharging time at a current density of 0.5 A g^{-1} for supercapacitors in the 1 M EMIMTFSI/LiTFSI/ACN electrolyte is the longest among the three types of organic electrolytes. And, its specific capacitance is up to 147 F g^{-1}. The energy density and power density of the UN-$Ti_3C_2T_x$ film electrode in the three electrolytes are displayed in the Ragone plots (Figure 4d). The device based on the EMIMTFSI/LiTFSI/ACN electrolyte achieves the highest energy density of 29.4 Wh kg^{-1} at the power density of 600 W kg^{-1}, and the highest power density of 1200 W kg^{-1} at the energy density of 20.77 Wh kg^{-1}.

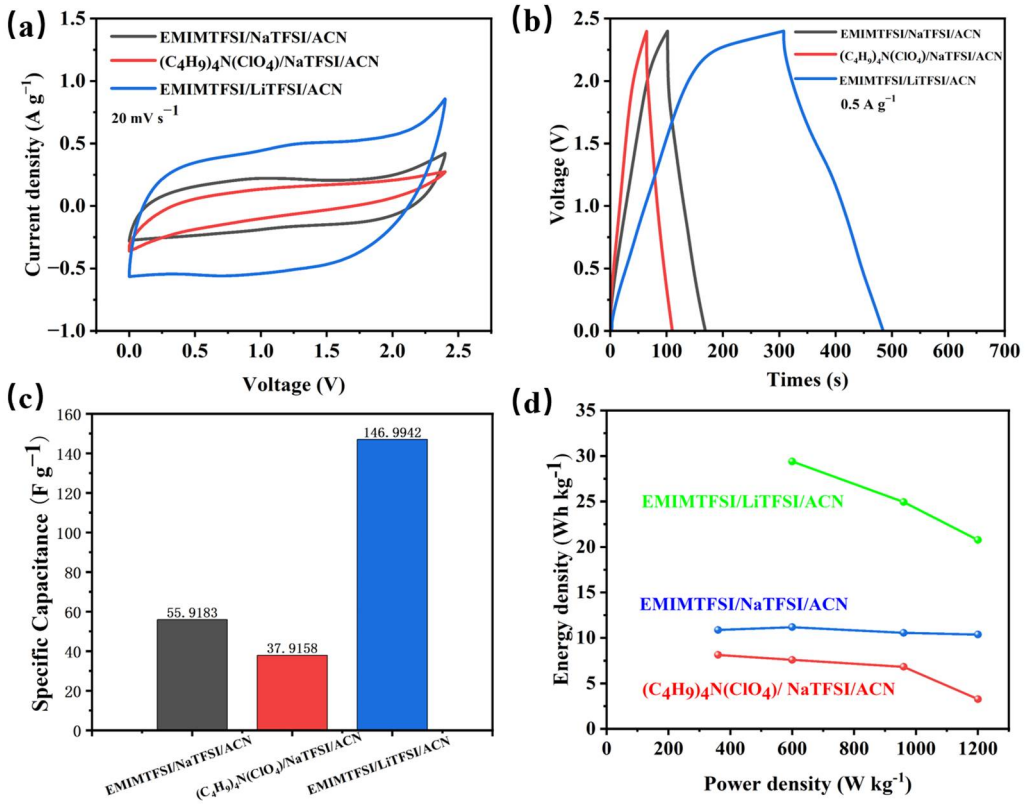


Figure 4. Electrochemical performance results in three types of electrolytes. (**a**) CV curves at a scan rate of 20 mV s^{-1}. (**b**) GCD curves at a current density of 0.5 A g^{-1}. (**c**) The gravimetric capacitances at a current density of 0.5 A g^{-1}. (**d**) Ragone plots of energy density versus power density.

For comparison, the previously reported electrochemical performance parameters of the MXene-based electrodes in different types of electrolytes are listed, as detailed in Table 1. In aqueous electrolytes, MXene-based electrodes usually exhibit a narrow voltage window, despite the fact that they (such as the Ni-MOF/MXene and A-MHA) have higher specific capacitance than the UN-MXene film electrode, however, the narrow voltage window indeed constrains the improvement of the energy density, while in organic electrolytes, MXene-based electrodes show a wider voltage window and display a higher energy density. It is also important to note that there are significant performance variations among the same electrode material and electrolyte combinations, which may be related to factors such as the microstructure and surface properties of the electrode material, as well as the interactions between the electrolyte and the electrode. Among them, the supercapacitor based on the 1 M EMIMTFSI/LiTFSI/ACN organic electrolyte exhibits the highest voltage window (2.4 V) and the most excellent energy density (29.4 Wh kg^{-1}). This work can increase the supercapacitor's energy density by optimizing the design of the organic ionic liquid electrolyte (by introducing smaller-sized lithium ions) to match the modified electrode, thereby obtaining good electrochemical performance.

To evaluate the electrochemical performance of the UN-$Ti_3C_2T_x$ film electrode in the 1 M EMIMTFSI/LiTFSI/ACN electrolyte, Figure 5a shows that all areas defined by CV curves increase with the increasing scan rate. Moreover, at a large scan rate, the redox peaks disappear, and the corresponding capacitance is due to pseudocapacitance. Figure 5b shows GCD curves of the UN-$Ti_3C_2T_x$ film electrode at different current densities. At slightly higher current densities, the GCD curves roughly exhibit the typical triangular shape. However, at 0.5 A g^{-1}, the GCD curves reflect that the charging time is longer than the discharging time, which is possibly due to the fact in the low current density, the charging process is affected by diffusion kinetics, surface reaction, and the intercalation process. At

0.5 A g^{-1}, the maximum specific capacitance of the UN-$Ti_3C_2T_x$ film electrode is 147 F g^{-1} and delivers an energy density of 29.4 Wh kg^{-1} at a power density of 600 W kg^{-1}. Even at the high power density of 1200 W kg^{-1}, the energy density still remains 20.77 Wh kg^{-1}.

Table 1. Reported performance data for MXene-doped electrodes.

Electrode	Electrolyte	Voltage Window	Specific Capacitance	Energy Density	Ref.
WO_3/MXene	1 M H_2SO_4	−0.5~0 V	290 F g^{-1} @ 1 A g^{-1}	14 Wh kg^{-1} @ 6000W kg^{-1}	[26]
MnO_2-MXene	1 M Na_2SO_4	0~1 V	165 F g^{-1} @ 0.5 A g^{-1}	20 Wh kg^{-1} @ 500 W kg^{-1}	[27]
MXene/CNTs	6 M KOH	0~0.6 V	55.3 F g^{-1} @ 0.5 A g^{-1}	2.77 Wh kg^{-1} @ 311 W kg^{-1}	[28]
MXene/HG	1 M H_2SO_4	−0.5~0.5 V	106.86 F g^{-1} @ 0.5 A g^{-1}	14.84 Wh kg^{-1} @ 250 W kg^{-1}	[29]
Ni-MOF/ MXene	1 M KOH	0~0.5 V	716.19 F g^{-1} @ 1 A g^{-1}	16.59 Wh kg^{-1} @ 4182 W kg^{1}	[30]
MXene-rGO	3 M H_2SO_4	0~0.6 V	347.6 F g^{-1} @ 2 mv s^{-1}	11. 7 Wh kg^{-1} @ 140.1 W kg^{1}	[31]
Aligned MXene hybrid aerogels (A-MHA)	1 M H_2SO_4	−0.45~0.35 V	760 F g^{-1} @ 1 A g^{-1}	5.2 Wh kg^{-1} @ 69.9 W kg^{1}	[32]
MXene/MWCNTs	1 M EMITFSI/ACN	−1.5~1.5 V	85 F g^{-1} @ 2 mv s^{-1}	-	[13]
MXene hydrogel	EMITFSI	0~3 V	70 F g^{-1} @ 20 mv s^{-1}	-	[14]
N-doped MXene	1 M $(C_4H_9)_4N(ClO_4)$/ NaTFSI/ACN	0~2.4 V	37.9 F g^{-1} @ 0.5 A g^{-1}	8.13 Wh kg^{-1} @ 360 W kg^{1}	This work
N-doped MXene	1 M EMIMTFSI/ NaTFSI/ACN	0~2.4 V	55.9 F g^{-1} @ 0.5 A g^{-1}	11.18 Wh kg^{-1} @ 600 W kg^{1}	This work
N-doped MXene	1 M EMIMTFSI/ LiTFSI/ACN	0~2.4 V	147 F g^{-1} @ 0.5 A g^{-1}	29.4 Wh kg^{-1} @ 600 W kg^{1}	This work

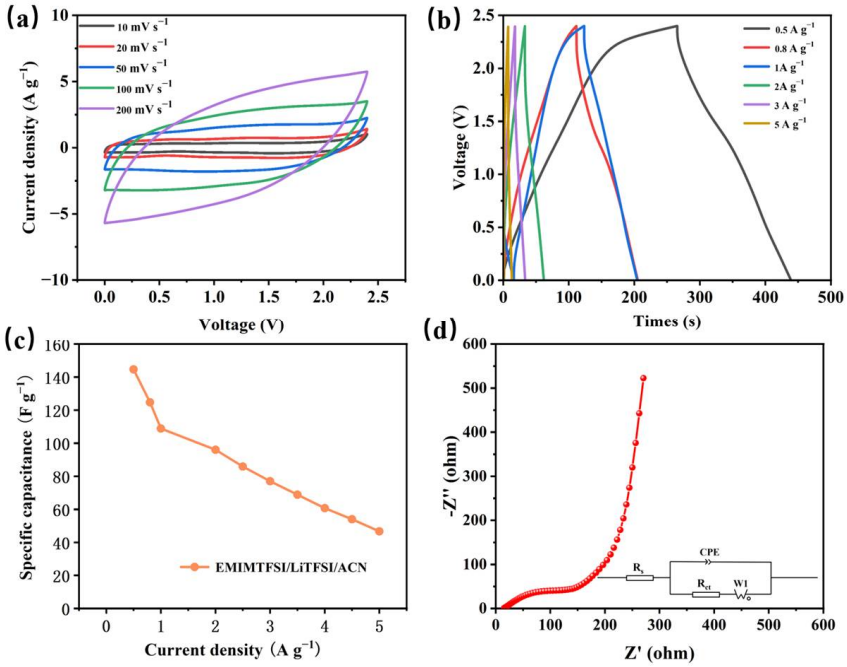


Figure 5. Electrochemical performance results in the 1 M EMIMTFSI/LiTFSI/ACN electrolyte. (**a**) CV curves of the UN-$Ti_3C_2T_x$ film electrode at different scan rates. (**b**) GCD curves of the UN-$Ti_3C_2T_x$ film electrode at different current densities, and (**c**) the corresponding capacitance. (**d**) Nyquist impedance plots of the UN-$Ti_3C_2T_x$ film electrode. The inset shows the equivalent circuit used to simulate the EIS spectrum.

Electrochemical impedance spectroscopy (EIS) can be used to analyze the dynamic behavior of electrons and ions, as shown in Figure 5d. The equivalent circuit used to simulate the EIS spectrum is shown in the inset of Figure 5d. The intersection of the semicircle and the X-axis is the contact resistance (R_s). The corresponding R_s value in the high-frequency region is 15.36 Ω, indicating that the as-fabricated device exhibits a higher R_s value compared to those reported for MXene-based electrodes, due to the influence of the ionic conductivity and the high viscosity of organic electrolytes. The R_{ct} is the charge transfer resistance, which is mainly related to the electrode porosity [33]. The ion size of organic ions ($EMIM^+$, $TFSI^-$) is large, thus limiting their migration within the UN-$Ti_3C_2T_x$ film electrodes, which increases the resistance to ion and molecule transport, leading to a large value for R_{ct}. The increased R_{ct} and R_s may also suggest that the electrode may not retain its capacitance over extended cycling, affecting the device's long-term stability. However, the straight line near 90° at a low frequency represents the Warburg impedance, indicating ideal electrochemical capacitive behavior.

4. Conclusions

In this work, we synthesized freestanding and compact N-doped delaminated d-$Ti_3C_2T_x$ (UN-$Ti_3C_2T_x$) film electrodes, and investigated their electrochemical performance in three different electrolytes, also including 1 M EMIMTFSI/NaTFSI/ACN, 1 M $(C_4H_9)_4N(ClO_4)$/NaTFSI/ACN, and 1 M EMIMTFSI/LiTFSI/ACN electrolytes, respectively. Among them, the supercapacitor based on the 1 M EMIMTFSI/LiTFSI/ACN electrolyte exhibits the best electrochemical performance due to the smaller ion size for Li^+ in the organic electrolyte. Also, the nitrogen-doped MXene electrodes effectively adjust the interlayer spacing of the MXene nanosheets, and the enlarged interlayer spacing (from 12.60 Å to 14.24 Å) is more favorable for the intercalation and de-intercalation of the larger-sized organic ions within the electrodes, thus effectively storing a charge. As a result, the supercapacitor based on nitrogen-doped MXene electrodes in the 1 M EMIMTFSI/LiTFSI/ACN electrolyte exhibits a high-voltage window of 2.4 V, and achieves the electrode capacitance of up to 147 F g^{-1}, with the maximum energy density of 29.4 Wh kg^{-1}. Therefore, by reasonably designing and optimizing ionic liquid electrolytes to match MXene-based electrode materials, it is feasible to achieve the supercapacitors with the highest performance.

Supplementary Materials: The following supporting information can be downloaded at: https://www.mdpi.com/article/10.3390/chemistry7010013/s1, Figure S1: XRD pattern of Ti_3AlC_2 powders; Figure S2: Cycling stability and Coulombic efficiency of UN-MXene electrode measured at 1 A g^{-1}; Table S1: XPS results of d-$Ti_3C_2T_x$ and UN-$Ti_3C_2T_x$ samples.

Author Contributions: Y.L.: Original draft, formal analysis, and investigation. X.B.: Conceptualization, review, and editing. J.X.: Review and editing. X.H.: Review and editing. W.Q.: Conceptualization, review, and editing. All authors have read and agreed to the published version of the manuscript.

Funding: This work was supported by the Key Science and Technology Developing Project of Shaanxi Province (2020KWZ-004) and the "Scientist + Engineer" Project of Shaanxi Province (No. 2022KXJ-162).

Data Availability Statement: The data that support the conclusions of this study are included in the article and Supplementary Materials.

Conflicts of Interest: The authors declare no conflicts of interest.

References

1. Feng, D.; Lei, T.; Lukatskaya, M.R.; Park, J.; Huang, Z.; Lee, M.; Shaw, L.; Chen, S.; Yakovenko, A.A.; Kulkarni, A.; et al. Robust and conductive two-dimensional metal-organic frameworks with exceptionally high volumetric and areal capacitance. *Nat. Energy* **2018**, *3*, 30–36. [CrossRef]
2. Shao, Y.; EI-Kady, M.F.; Sun, J.; Li, Y.; Zhang, Q.; Zhu, M.; Wang, H.; Dunn, B.; Kaner, R.B. Design and Mechanisms of Asymmetric Supercapacitors. *Chem. Rev.* **2018**, *118*, 9233–9280. [CrossRef]
3. Lukatskaya, M.R.; Bruce, D.; Yury, G. Multidimensional materials and device architectures for future hybrid energy storage. *Nat. Commun.* **2016**, *7*, 12647. [CrossRef] [PubMed]
4. Michael, N.; Murat, K.; Volker, P.; Lu, J.; Niu, J.; Heon, M.; Hultman, L.; Gogotsi, Y.; Barsoum, M.W. Two-dimensional nanocrystals produced by exfoliation of Ti_3AlC_2. *Adv. Mater.* **2011**, *23*, 4248–4253.
5. Lukatskaya, M.R.; Mashtalir, O.; Ren, E.C.; Dall'agnese, Y.; Rozier, P.; Taberna, P.L.; Naguib, M.; Simon, P.; Barsoum, M.W.; Gogotsi, Y. Cation Intercalation and High Volumetric Capacitance of Two-Dimensional Titanium Carbide. *Science* **2013**, *341*, 1502–1505. [CrossRef] [PubMed]
6. Hart, J.L.; Kanit, H.; Lang, A.C.; Anasori, B.; Pinto, D.; Pivak, Y.; van Omme, J.T.; May, S.J.; Gogotsi, Y.; Taheri, M.L. Control of MXenes' electronic properties through termination and intercalation. *Nat. Commun.* **2019**, *10*, 522. [CrossRef]
7. Lukatskaya, M.R.; Kota, S.; Lin, Z.; Zhao, M.-Q.; Shpigel, N.; Levi, M.D.; Halim, J.; Taberna, P.-L.; Barsoum, M.W.; Simon, P.; et al. Ultra-high-rate pseudocapacitive energy storage in two-dimensional transition metal carbides. *Nat. Energy* **2017**, *2*, 12647–12854. [CrossRef]
8. Wang, Z.; Zhong, X.; Huang, H.; Chu, X.; Xie, Y.; Xiong, D.; Yan, C.; Zhao, H.; Zhang, H.; Yang, W. Unraveling and Regulating Self-Discharge Behavior of Ti_3C2T_x MXene-Based Supercapacitors. *ACS Nano* **2020**, *14*, 4916–4924. [CrossRef] [PubMed]
9. Shi, X.; Zhang, W.; Wang, J.; Zheng, W.; Huang, K.; Zhang, H.; Feng, S.; Chen, H. $(EMIm)^+$ $(PF6)^-$ ionic liquid unlocks optimum energy/power density for architecture of nanocarbon-based dual-ion battery. *Adv. Energy Mater.* **2016**, *6*, 1601378. [CrossRef]
10. Lei, Z.; Chen, B.; Koo, Y.; MacFarlane, D. Introduction: Ionic Liquids. *Chem. Rev.* **2017**, *117*, 6633–6635. [CrossRef]
11. Bag, S.; Samanta, A.; Bhunia, P.; Raj, C.R. Rational functionalization of reduced graphene oxide with imidazolium-based ionic liquid for supercapacitor application. *Int. J. Hydrogen Energy* **2016**, *41*, 22134–22143. [CrossRef]
12. Zhou, H.; Sun, W.; Li, J. Preparation of spiro-type quaternary ammonium salt via economical and efficient synthetic route as electrolyte for electric double-layer capacitor. *J. Cent. South Univ.* **2015**, *22*, 2435–2439. [CrossRef]
13. Dall'Agnese, Y.; Rozier, P.; Taberna, P.; Gogotsi, Y.; Simon, P. Capacitance of two-dimensional titanium carbide (MXene) and MXene/carbon nanotube composites in organic electrolytes. *J. Power Sources* **2016**, *306*, 510–515. [CrossRef]
14. Lin, Z.; Barbara, D.; Taberna, P.; Van Aken, K.L.; Anasori, B.; Gogotsi, Y.; Simon, P. Capacitance of $Ti_3C_2T_x$ MXene in ionic liquid electrolyte. *J. Power Sources* **2016**, *326*, 575–579. [CrossRef]
15. Lin, Z.; Rozier, P.; Duployer, B.; Taberna, P.L.; Anasori, B.; Gogotsi, Y.; Simon, P. Electrochemical and in-situ X-ray diffraction studies of $Ti_3C_2T_x$ MXene in ionic liquid electrolyte. *Electrochem. Commun.* **2016**, *72*, 50–53. [CrossRef]
16. Liang, K.; Matsumoto, R.A.; Zhao, W.; Osti, N.C.; Popov, I.; Thapaliya, B.P.; Fleischmann, S.; Misra, S.; Prenger, K.; Tyagi, M.; et al. Engineering the Interlayer Spacing by Pre-Intercalation for High Performance Supercapacitor MXene Electrodes in Room Temperature Ionic Liquid. *Adv. Funct. Mater.* **2021**, *31*, 2104007. [CrossRef]
17. Gandla, D.; Zhang, F.; Tan, D. Advantage of Larger Interlayer Spacing of a $Mo_2Ti_2C_3$ MXene Free-Standing Film Electrode toward an Excellent Performance Supercapacitor in a Binary Ionic Liquid-Organic Electrolyte. *J. Am. Chem. Soc.* **2022**, *7*, 7190–7198. [CrossRef] [PubMed]
18. Masashi, O.; Akira, S.; Satoshi, K.; Yamada, A. MXene as a Charge Storage Host. *Acc. Chem. Res.* **2018**, *51*, 591–599.
19. Sun, L.; Zhuo, K.; Chen, Y.; Du, Q.; Zhang, S.; Wang, J. Ionic Liquid-Based Redox Active Electrolytes for Supercapacitors. *Adv. Funct. Mater.* **2022**, *32*, 2203611. [CrossRef]
20. Lu, C.; Li, Y.; Yan, B.; Sun, L.; Zhang, P.; Zhang, W.; Sun, Z.M. Nitrogen-Doped Ti_3C_2 MXene: Mechanism Investigation and Electrochemical Analysis. *Adv. Funct. Mater.* **2020**, *30*, 2000852. [CrossRef]
21. Yang, C.; Tang, Y.; Tian, Y.; Luo, Y.; Din, M.F.U.; Yin, X.; Que, W. Flexible Nitrogen-Doped 2D Titanium Carbides (MXene) Films Constructed by an Ex Situ Solvothermal Method with Extraordinary Volumetric Capacitance. *Adv. Energy Mater.* **2018**, *8*, 1802087. [CrossRef]
22. Naguib, M.; Come, J.; Dyatkin, B.; Presser, V.; Taberna, P.-L.; Simon, P.; Barsoum, M.W.; Gogotsi, Y. MXene: A promising transition metal carbide anode for lithium-ion batteries. *Electrochem. Commun.* **2012**, *16*, 61–64. [CrossRef]
23. Yang, C.; Tang, Y.; Tian, Y.; Luo, Y.; Yin, X.; Que, W. Methanol and Diethanolamine Assisted Synthesis of Flexible Nitrogen-Doped Ti_3C_2 (MXene) Film for Ultrahigh Volumetric Performance Supercapacitor Electrodes. *ACS Appl. Energy Mater.* **2019**, *3*, 586–596. [CrossRef]
24. Dall'Agnese, Y.; Lukatskaya, R.M.; Cook, M.K.; Taberna, P.L.; Gogotsi, Y.; Simon, P. High capacitance of surface-modified 2D titanium carbide in acidic electrolyte. *Electrochem. Commun.* **2014**, *481*, 18–22. [CrossRef]

25. Xie, Y.; Chen, G.; Tang, Y.; Wang, Z.; Zhou, J.; Bi, Z.; Xuan, X.; Zou, J.; Zhang, A.; Yang, C. Unraveling the Ionic Storage Mechanism of FlexibleNitrogen-Doped MXene Films for High-PerformanceAqueous Hybrid Supercapacitors. *Small* **2024**, *20*, 2405817. [CrossRef] [PubMed]
26. Nishad, H.; Mane, M.; Patole, P.; Lee, J.; Gosavi, S.; Walke, P.S. Temperature driven pseudocapactive performance of WO_3/MXene nanocomposite for asymmetric aqueous supercapacitors. *Chem. Eng. J.* **2024**, *495*, 153360. [CrossRef]
27. Zhu, Y.; Rajouâ, K.; Vot, L.S.; Fontaine, O.; Simon, P.; Favier, F. MnO_2-MXene Composite as Electrode for Supercapacitor. *J. Electrochem. Soc.* **2022**, *169*, 0305524. [CrossRef]
28. Yang, L.; Zheng, W.; Zhang, P.; Chen, J.; Tian, W.; Zhang, Y.; Sun, Z. MXene/CNTs films prepared by electrophoretic deposition for supercapacitor electrodes. *J. Electroanal. Chem.* **2018**, *830*, 1–6. [CrossRef]
29. Cai, Z.; Ma, Y.; Wang, M.; Qian, A.N.; Tong, Z.M.; Xiao, L.T.; Jia, S.T.; Chen, X.Y. Engineering of electrolyte ion channels in MXene/holey graphene electrodes for superior supercapacitive performances. *Rare Met.* **2022**, *41*, 2084–2093. [CrossRef]
30. Shivade, S.; Kurade, N.; Bhosale, K.; Kundale, S.S.; Shelake, A.R.; Patil, A.D.; Waifalkar, P.P.; Kamat, R.K.; Teli, A.M.; Dongale, T.D. Folic acid-assisted in situ solvothermal synthesis of Ni-MOF/MXene composite for high-performance supercapacitors. *J. Energy Storage* **2024**, *100*, 113754. [CrossRef]
31. Li, P.; Guan, G.; Shi, X.; Lu, L.; Fan, Y.C.; Xu, J.; Shang, Y.Y.; Zhang, Y.J.; Wei, J.Q.; Guo, F.M. Bidirectionally aligned MXene hybrid aerogels assembled with MXene nanosheets and microgels for supercapacitors. *Rare Met.* **2023**, *42*, 1249–1260. [CrossRef]
32. Liu, Z.; Xue, F.; Zhao, X.; Chen, Z.; Zheng, H.; Ding, R.; Li, P.; Xu, L.; Xiong, J.; Peng, Q.; et al. Anti-stacking synthesis of MXene-reduced graphene oxide sponges for aqueous zinc-ion hybrid supercapacitor with improved performance. *J. Mater. Sci. Technol.* **2023**, *154*, 22–29. [CrossRef]
33. Huang, Y.; Liang, J.; Chen, Y. An overview of the applications of graphene-based materials in supercapacitors. *Small* **2012**, *8*, 1805–1834. [CrossRef] [PubMed]

Disclaimer/Publisher's Note: The statements, opinions and data contained in all publications are solely those of the individual author(s) and contributor(s) and not of MDPI and/or the editor(s). MDPI and/or the editor(s) disclaim responsibility for any injury to people or property resulting from any ideas, methods, instructions or products referred to in the content.